



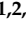




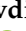







Article

Search for double beta decay of ^{106}Cd with an enriched $^{106}\text{CdWO}_4$ crystal scintillator in coincidence with CdWO_4 scintillation counters

P. Belli^{1,2} , R. Bernabei^{1,2*} , V.B. Brudanin³ , F. Cappella^{4,5} , V. Caracciolo^{1,2,6} , R. Cerulli^{1,2} , F.A. Danevich⁷ , A. Incicchitti^{4,5} , D.V. Kasperovych⁷ , V.R. Klavdiienko⁷ , V.V. Kobychyev⁷ , V. Merlo^{1,2} , O.G. Polischuk⁷ , V.I. Tretyak⁷  and M.M. Zarytskyi⁷ 

¹ INFN, sezione di Roma "Tor Vergata", I-00133 Rome, Italy

² Dipartimento di Fisica, Università di Roma "Tor Vergata", I-00133 Rome, Italy

³ Joint Institute for Nuclear Research, 141980 Dubna, Russia

⁴ INFN, sezione Roma "La Sapienza", I-00185 Rome, Italy

⁵ Dipartimento di Fisica, Università di Roma "La Sapienza", I-00185 Rome, Italy

⁶ INFN, Laboratori Nazionali del Gran Sasso, 67100 Assergi (AQ), Italy

⁷ Institute for Nuclear Research of NASU, 03028 Kyiv, Ukraine

* Correspondence: Dipartimento di Fisica, Università di Roma "Tor Vergata", I-00133 Rome, Italy. E-mail address: rita.bernabei@roma2.infn.it (Rita Bernabei)

Received: date; Accepted: date; Published: date

Abstract: Studies on double beta decay processes in ^{106}Cd were performed by using a cadmium tungstate scintillator enriched in ^{106}Cd at 66% ($^{106}\text{CdWO}_4$) with two CdWO_4 scintillation counters (with natural Cd composition). No effect was observed in the data accumulated over 26033 h. New improved half-life limits were set on the different channels and modes of the ^{106}Cd double beta decay at level of $\lim T_{1/2} \sim 10^{20} - 10^{22}$ yr. The limit for the two neutrino electron capture with positron emission in ^{106}Cd to the ground state of ^{106}Pd , $T_{1/2}^{2\nu\text{EC}\beta^+} \geq 2.1 \times 10^{21}$ yr, was set by the analysis of the $^{106}\text{CdWO}_4$ data in coincidence with the energy release 511 keV in both CdWO_4 counters. The sensitivity approaches the theoretical predictions for the decay half-life that are in the range $T_{1/2} \sim 10^{21} - 10^{22}$ yr. The resonant neutrinoless double-electron capture to the 2718 keV excited state of ^{106}Pd is restricted at the level of $T_{1/2}^{0\nu 2K} \geq 2.9 \times 10^{21}$ yr.

Keywords: Double beta decay; ^{106}Cd ; Scintillation detector; Low background experiment

1. Introduction

Observations of the neutrino oscillations suggest that the neutrinos are massive, which calls for extension of the Standard Model of particles and fields (SM). However, oscillation experiments cannot determine the neutrino mass and the neutrino mass hierarchy. One of the most promising tools to determine the absolute neutrino mass scale and the neutrino mass hierarchy, the nature of the neutrino (Dirac or Majorana particle?), to check the lepton number conservation is double beta (2β) decay of atomic nuclei, a process in which two electrons (or positrons) are emitted simultaneously and nuclear charge changes by two units: $(A, Z) \rightarrow (A, Z \pm 2)$ [1–3]. The neutrinoless mode of the decay ($0\nu 2\beta$) violates the lepton number conservation law and it is possible if the neutrinos are Majorana particles (particle is equal to its antiparticle). Being a process beyond the SM, the $0\nu 2\beta$ decay has the potential to test the SM [4–6]. Moreover, the Majorana nature of the neutrino might shed light on the Universe baryon asymmetry problem [7,8].

The two-neutrino 2β decay ($2\nu 2\beta$) is a radioactive process allowed in the SM with the longest half-lives ever observed: $10^{18} - 10^{24}$ yr. The $2\nu 2\beta^-$ decay mode has been detected in several nuclides [9].

The $0\nu 2\beta$ decay is not observed. The most sensitive $2\beta^-$ -decay experiments quote half-life limits at level of $T_{1/2} > (10^{24} - 10^{26})$ yr, which correspond to Majorana neutrino mass limits in the range $\langle m_\nu \rangle < (0.1 - 0.7)$ eV. Probing the inverted hierarchy region of the neutrino mass requires improved sensitivities of $2\beta^-$ experiments at level of $\langle m_\nu \rangle \sim (0.02 - 0.05)$ eV (i.e. half-life sensitivity in the range: $T_{1/2} \sim 10^{27} - 10^{28}$ yr).

The sensitivity of the experiments in the search for “double beta plus” processes: double electron capture (2EC), electron capture with positron emission ($EC\beta^+$) and double positron decay ($2\beta^+$) is substantially lower, while the physical lepton-number violating mechanisms of the neutrinoless 2EC, $EC\beta^+$ and $2\beta^+$ processes are considered essentially the same as for the decay with electrons emission. At the same time, there is a motivation to search for the $0\nu EC\beta^+$ and $0\nu 2\beta^+$ decays owing to the potential to clarify the possible contribution of the right-handed currents to the $0\nu 2\beta^-$ decay rate [10], and an interesting possibility of a resonant $0\nu 2EC$ process [11–14].

As for the allowed two-neutrino mode of the double beta plus decay, there are claims of positive results (indication) for the $2\nu 2EC$ radioactivity of three nuclides. The $2\nu 2EC$ decay of ^{130}Ba was claimed in two geochemical experiments where anomaly in the isotopic concentrations of daughter xenon traces in old barite (BaSO_4) minerals was interpreted as the sought effect with the half-life $T_{1/2} = (2.16 \pm 0.52) \times 10^{21}$ yr [15], and with $T_{1/2} = (6.0 \pm 1.1) \times 10^{20}$ yr in [16]. In the analysis [17] the disagreement was explained by a possible cosmogenic contribution with a conclusion that the result of [15] is a more reliable one. An indication on the $2\nu 2EC$ process in ^{78}Kr with the half-life $T_{1/2} = 9.2_{-2.9}^{+5.7} \times 10^{21}$ yr was obtained with a proportional counter with a volume of 49 lt filled by gas enriched in ^{78}Kr to 99.81% [18]. The value was then updated to $1.9_{-0.8}^{+1.3} \times 10^{22}$ yr in [19]. Recently a detection of the $2\nu 2EC$ of ^{124}Xe with the half-life $(1.8 \pm 0.5) \times 10^{22}$ yr was claimed in [20]. However, the indications of ^{130}Ba 2EC decay should be confirmed in direct counting experiments, while the results for ^{78}Kr and ^{124}Xe need to be confirmed with bigger statistics and very stable experiments. Other allowed 2ν decay channels with decrease of the nuclear charge by two units, $2\nu EC\beta^+$ and $2\nu 2\beta^+$, are not observed yet.

The nuclide ^{106}Cd is one of the most appealing candidates to search for 2EC, $EC\beta^+$ and $2\beta^+$ decays with a long history of studies (a review of the previous investigations reader can find in Ref. [21]). The interest to ^{106}Cd can be explained by one of the biggest decay energy $Q_{2\beta} = 2775.39(10)$ keV [22], comparatively high isotopic abundance $\delta = 1.245(22)\%$ [23] and possibility of gas centrifugation for enrichment, existing technologies of cadmium purification, availability of Cd-containing detectors to realize calorimetric experiments with a high detection efficiency.

At present there are three running experiments searching for the double beta decay of ^{106}Cd : COBRA, TGV-2 and the present one.

The COBRA collaboration utilizes CdZnTe semiconductor detectors at the Gran Sasso underground laboratory (Laboratori Nazionali del Gran Sasso, LNGS). The experiment started with one $\text{Cd}_{0.9}\text{Zn}_{0.1}\text{Te}$ detector with mass of $\simeq 3$ g, and one CdTe detector ($\simeq 6$ g) [24]. CdZnTe detectors are used in the current stage of the experiment [25,26]. The measurements resulted in the half-life limits for several channels of ^{106}Cd double beta decay at level of $\sim 10^{18}$ yr.

The main goal of the TGV-2 experiment, located at the Modane underground laboratory, is search for $2\nu 2EC$ decay of ^{106}Cd (a decay channel expected to be the fastest one) with the help of 32 planar HPGe detectors with a total sensitive volume ≈ 400 cm³. In the first stage of the experiment, foils of cadmium enriched in ^{106}Cd to (60–75)% were used [27–29]; now 23.2 g of cadmium sample enriched in ^{106}Cd to 99.57% are installed in the set-up [30]. The experiment gives the strongest limit on the $2\nu 2EC$ decay: $T_{1/2} > 4.7 \times 10^{20}$ yr. For other decay modes and channels the sensitivity is at level of 10^{20} yr [31].

A cadmium tungstate crystal scintillator from cadmium enriched in ^{106}Cd to 66% ($^{106}\text{CdWO}_4$) was developed in 2010 [32]. The experiments with that detector are carried out at the LNGS in the DAMA/CRYSTAL, DAMA/R&D set-ups, and in an ultra-low background GeMulti HPGe γ spectrometer of

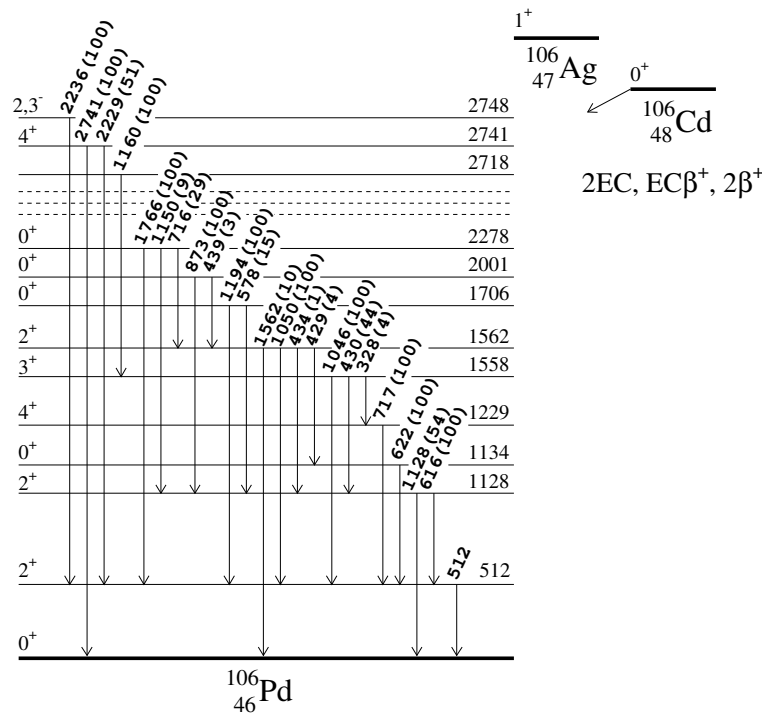


Figure 1. Simplified decay scheme of ^{106}Cd [36] (levels with energies in the energy interval (2283–2714) keV are omitted). Energies of the excited levels are in keV. Relative intensities of γ quanta are given in parentheses.

the STELLA (SubTERRanean Low Level Assay) facility [33] at the LNGS. The first stage of the experiment with the $^{106}\text{CdWO}_4$ detector gave the half-life limits on 2β processes in ^{106}Cd at level of $\sim 10^{20}$ yr [21]. In the second stage the $^{106}\text{CdWO}_4$ scintillator was installed between four HPGe detectors (with volume $\simeq 225$ cm³ each) of the GeMulti HPGe γ spectrometer to detect γ quanta expected in the most of the ^{106}Cd decay channels, including the annihilation γ 's emitted in decay modes with positron(s) emission (a simplified decay scheme of ^{106}Cd is presented in Fig. 1). The experiment improved the ^{106}Cd half-life limits to the level of $T_{1/2} \geq (10^{20} - 10^{21})$ yr [34]. In the third stage, described in the present report, the $^{106}\text{CdWO}_4$ detector was running in coincidence (anti-coincidence) with two large volume CdWO_4 crystal scintillators in a close geometry to increase the detection efficiency to γ quanta expected to be emitted from the $^{106}\text{CdWO}_4$ crystal in the double beta decay processes in ^{106}Cd . Preliminary results of the experiment stage were reported in [35].

2. The experiment

The $^{106}\text{CdWO}_4$ crystal scintillator of roughly cylindrical shape (approximate sizes $\varnothing 27$ mm \times 50 mm, mass 215.4 g) was viewed by a 3 inches low radioactive photo-multiplier tube (PMT) Hamamatsu R6233MOD through a lead tungstate (PbWO_4) crystal light-guide ($\varnothing 40$ mm \times 83 mm). The PbWO_4 crystal has been developed from the highly purified [37] archaeological lead [38]. Two CdWO_4 crystal scintillators $\varnothing 70$ mm \times 38 mm include a cylindrical cut-out to house the $^{106}\text{CdWO}_4$ crystal. They were viewed by two 3 inches low radioactive PMTs EMI9265B53/FL through light-guides glued in two parts: low radioactive quartz ($\varnothing 66$ mm \times 100 mm, close to the CdWO_4 scintillators) and optical quality polystyrene ($\varnothing 66$ mm \times 100 mm). A schematic of the set-up is shown in Fig. 2. The detector system was surrounded by four high purity copper bricks (referred hereinafter as “internal copper”) and by layers of high purity copper

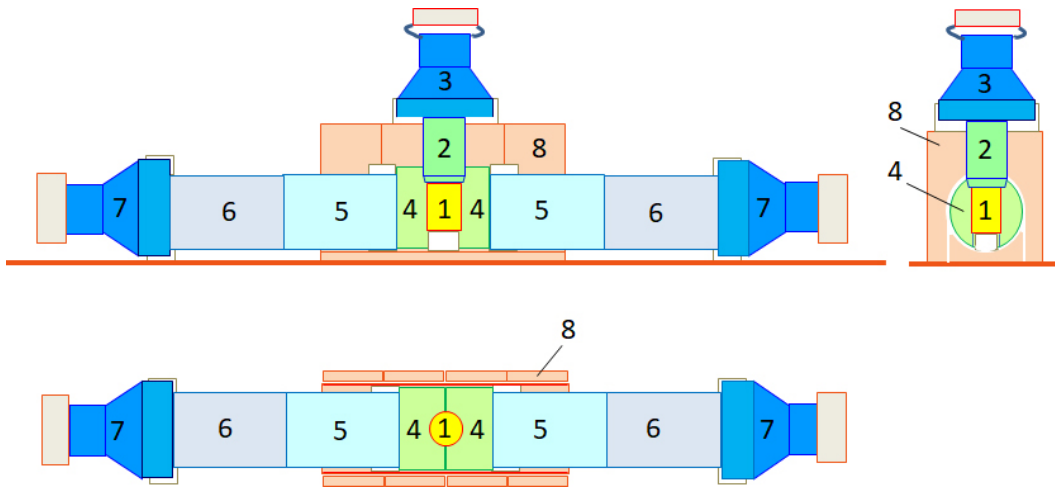


Figure 2. Schematic of the experimental set-up with the $^{106}\text{CdWO}_4$ scintillation detector. $^{106}\text{CdWO}_4$ crystal scintillator (1) is viewed through PbWO_4 light-guide (2) by photo-multiplier tube (3). Two CdWO_4 crystal scintillators (4) are viewed through light-guides glued from quartz (5) and polystyrene (6) by photo-multiplier tubes (7). The detector system was surrounded by passive shield made from copper, lead, polyethylene and cadmium (not shown). Only part of the copper details (8, “internal copper”), used to reduce the direct hits of the detectors by γ quanta from the PMTs, are shown.

(11 cm, referred hereinafter as “external copper”), low radioactive lead (10 cm), cadmium (2 mm) and polyethylene (10 cm) to reduce the external background. The inner volume of the set-up with the detector system was continuously flushed by high-purity nitrogen gas to remove environmental radon. The grade of the high-purity N_2 gas is at least 5.5 for what concerns the presence of other possible gases. However, the possible presence in trace of Radon gas in the Nitrogen atmosphere inside the copper box, housing the detector, has been checked with another set-up, by searching for the double coincidences of the γ -rays (609 and 1120 keV) from ^{214}Bi Radon daughter. The obtained upper limit on the possible Radon concentration in the high-purity Nitrogen atmosphere has been measured to be: $< 5.8 \times 10^{-2} \text{ Bq/m}^3$ (90% C.L.) [39]. Photographs of the detector system are shown in Fig. 3.

An event-by-event data acquisition system based on a 100 MS/s 14 bit transient digitizer (DT5724 by CAEN) recorded the amplitude, the arrival time and the pulse shape of each event. To reduce the data volume due to presence in the $^{106}\text{CdWO}_4$ crystal of ^{113}Cd and ^{113m}Cd β active nuclides [21,32], the energy threshold for the set-up was set at level of ≈ 510 keV for the anti-coincidence mode, while the energy threshold of the $^{106}\text{CdWO}_4$ detector in the coincidence with the CdWO_4 counters was ≈ 200 keV. The energy thresholds of the CdWO_4 counters were ≈ 70 keV. The energy scale and the energy resolution of the detectors were measured with ^{22}Na , ^{60}Co , ^{133}Ba , ^{137}Cs , and ^{228}Th γ sources at the beginning, in the middle, and at the end of the experiment.

The energy resolution of the $^{106}\text{CdWO}_4$ detector for the total exposure can be described by the function $\text{FWHM} = 6.85 \times \sqrt{E_\gamma}$, where FWHM (full width at half maximum) and E_γ are given in keV. The poor energy resolution of the enriched detector (despite excellent optical properties of the material [32]) is caused by the elongated shape of the enriched scintillator that results in a rather low and non-uniform light collection, and by using of not perfectly transparent PbWO_4 crystal light-guide. The performance of the CdWO_4 counters is substantially better. The energy spectra accumulated by one of the counters with ^{22}Na , ^{60}Co and ^{228}Th γ sources are presented in Fig. 4. The energy resolution of the counters was estimated by using the results of the three energy calibration campaigns as $\text{FWHM} = a \times \sqrt{E_\gamma}$ with the

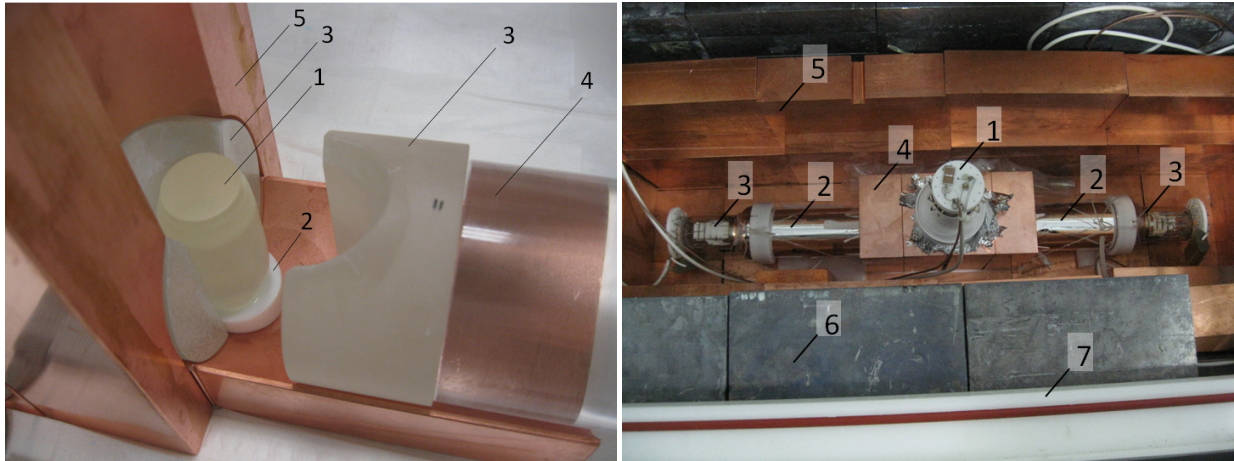


Figure 3. Left photograph: the $^{106}\text{CdWO}_4$ crystal scintillator (1), Teflon support of the $^{106}\text{CdWO}_4$ crystal (2), CdWO_4 crystal scintillators (3), quartz light-guide (4), “internal copper” brick (5). Right photograph: the detector system installed in the passive shield: PMT of the $^{106}\text{CdWO}_4$ detector (1), light-guides of the CdWO_4 counters wrapped by reflecting foil (2), PMT of the CdWO_4 counters (3), “internal copper” bricks (4), “external copper” bricks (5), lead bricks (6), polyethylene shield (7). The copper, lead and polyethylene shields are not completed.

coefficient a equal to 2.97 and 3.13 for the two detectors. The resolution formulas take into account also energy scale shifts during the data taking over the experiment.

Energy spectra of ^{22}Na source were simulated by the EGSnrc code [40]. The data measured with ^{22}Na source without coincidence selection and in coincidence with energy 511 keV in at least one of the CdWO_4 counters is compared with the simulated distribution in Fig. 5. The experimental data is in a reasonable agreement with the results of simulations.

A distribution of the $^{106}\text{CdWO}_4$ detector pulses start positions relative to the CdWO_4 signals with energy 511 keV is shown in Inset of Fig. 5. The time resolution of the detector system is rather high (the standard deviation of the distribution is 16 ns) due to the fast rise time of the CdWO_4 scintillation pulses.

3. Results and Discussion

3.1. Backgrounds reduction and model of the backgrounds

The difference in CdWO_4 scintillation pulse shape for β particles (γ quanta) and α particles can be used to suppress the background caused by α radioactive contamination of the detector due to the residual contamination in ^{232}Th and ^{238}U with their daughters. The mean time method was applied to the data to discriminate signals of different origin by pulse shape. For each signal $f(t)$, the numerical characteristic of its shape (mean time, ζ) was defined by using the following equation:

$$\zeta = \frac{\sum f(t_k) \cdot t_k}{\sum f(t_k)}, \quad (1)$$

where the sum is over the time channels k , starting from the origin of signal up to $35 \mu\text{s}$; $f(t_k)$ is the digitized amplitude (at the time t_k) of a given signal. The energy dependence of the parameter ζ and its standard deviation (the distributions of ζ for β particles (γ quanta) and α particles are well described by a Gaussian function) was determined by using the data of the calibration measurements with ^{228}Th gamma source. The obtained parameters were then used to discriminate β (γ) events from α events in the data of

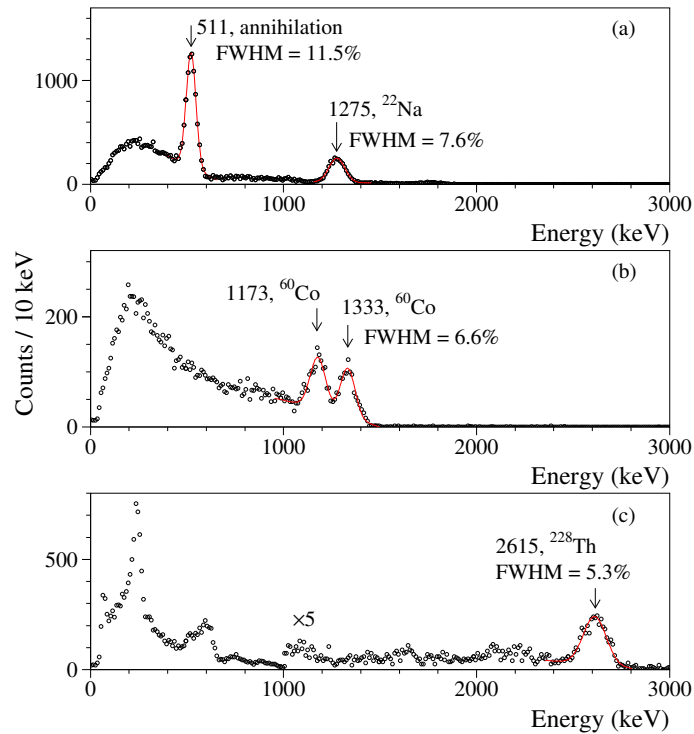


Figure 4. Energy spectra of ^{22}Na (a), ^{60}Co (b) and ^{228}Th (c) γ quanta measured by one of the CdWO_4 detectors. Fits of intensive γ peaks by Gaussian functions are shown by solid lines. Energies of γ quanta are in keV.

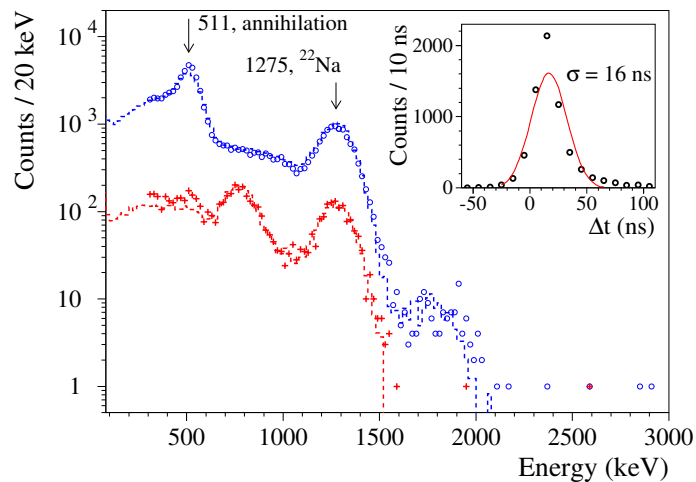


Figure 5. Energy spectra of ^{22}Na γ quanta measured by the $^{106}\text{CdWO}_4$ detector: with no coincidence cuts (blue circles) and in coincidence with energy 511 keV in at least one of the CdWO_4 counters (red crosses). The data simulated by using the EGSnrc Monte Carlo code are drawn by dashed lines. (Inset) Distribution of the $^{106}\text{CdWO}_4$ detector pulses start positions relative to the CdWO_4 signals with the energy 511 keV.

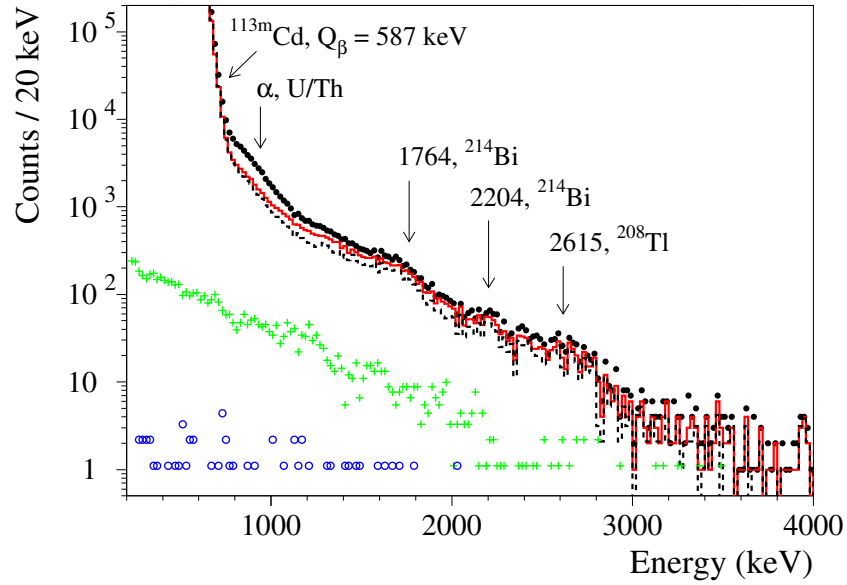


Figure 6. Energy spectra measured by the $^{106}\text{CdWO}_4$ detector for 26033 h in the low-background set-up without selection cuts (black dots), after selection of γ and β events by PSD using the mean time method (solid red line), the γ and β events in anti-coincidence with the CdWO_4 counters (dashed black line), the γ and β events in coincidence with event(s) in at least one of the CdWO_4 counters with the energy $E = 511 \pm 2\sigma$ keV (green crosses), the γ and β events in coincidence with events in both the CdWO_4 counters with the energy $E = 511 \pm 2\sigma$ keV (blue circles).

the low-background experiment. We refer reader to our previous works [21,34] where the pulse-shape discrimination (PSD) method was described in detail.

By using the PSD the α events were statistically separated from γ (β) events. In addition the method discarded from the data events of the $^{212}\text{Bi} - ^{212}\text{Po}$ sub-chain from the ^{232}Th family (due to the short decay time of $^{212}\text{Po} \approx 0.3 \mu\text{s}$ these decays are treated by the data acquisition system as a single event), PMT noise, pile-ups of signals in the $^{106}\text{CdWO}_4$ detector, $^{106}\text{CdWO}_4$ plus PbWO_4 events, etc. The results of the PSD method application to the background data gathered for 26033 h in the low-background set-up is shown in Fig. 6. The mean time method reduced the background mainly in the energy region (800–1300) keV (by a factor ~ 1.6) where α events of the ^{232}Th and ^{238}U with their daughters are expected.

Further reduction of the background counting rate (by a factor ~ 1.3 in the energy interval (1000–3000) keV) was achieved by exploiting the anti-coincidence with the CdWO_4 counters. The background was suppressed significantly by selection of events in the $^{106}\text{CdWO}_4$ detector in coincidence with the event(s) in at least one of the CdWO_4 counters with the energy release $E = 511 \pm 2\sigma$ keV (by a factor ~ 17 in the same energy interval; here σ is the energy resolution of the CdWO_4 counters for 511 keV γ quanta), and by selection of events in coincidence with the events in both the CdWO_4 counters with the energy $E = 511 \pm 2\sigma$ keV (by a further factor ~ 42). The stages of the background spectra reduction are presented in Fig. 6.

The counting rate of the $^{106}\text{CdWO}_4$ detector below the energy of ~ 0.8 MeV is mainly caused by the β decay of ^{113}Cd with the energy $Q_\beta = 323.83(27)$ keV [22] and of $^{113\text{m}}\text{Cd}$ ($Q_\beta = 587.37(27)$ keV [22,41]). A background model to describe the experimental data after the $^{113\text{m}}\text{Cd}$ β spectrum was constructed from distributions of “internal” (radioactive contamination of the $^{106}\text{CdWO}_4$ crystal) and “external” (radioactive contamination of the set-up details) sources. The equilibrium of the ^{238}U and ^{232}Th chains in all the

Table 1. Radioactive contamination (mBq/kg) of the materials of the low-background set-up estimated by using the fit of the energy spectra presented in Fig. 7. Upper limits are given at 68% C.L.

Material	^{40}K	^{56}Co	^{60}Co	^{88}Y	^{210}Pb	^{226}Ra	^{228}Ac	^{228}Th
PbWO ₄ crystal	≤ 0.09	–	–	–	$\leq 12 \times 10^3$	≤ 0.07	≤ 0.28	≤ 0.23
CdWO ₄ crystals	–	–	–	–	–	≤ 0.27	–	≤ 0.014
Quartz light-guides	≤ 18	–	–	–	–	≤ 3.3	≤ 0.6	≤ 0.6
Copper internal	≤ 0.8	≤ 0.26	≤ 0.5	≤ 0.005	–	≤ 3.0	≤ 1.3	≤ 0.019
Copper external	≤ 1.4	–	–	–	–	≤ 1.5	≤ 3.2	≤ 0.026
PMTs	≤ 1060	–	–	–	–	≤ 140	≤ 1030	≤ 250

materials is assumed to be broken¹. The sub-chains $^{228}\text{Ra} \rightarrow ^{228}\text{Th}$, $^{228}\text{Th} \rightarrow ^{208}\text{Pb}$ (the ^{232}Th family) and $^{238}\text{U} \rightarrow ^{234}\text{U}$, $^{226}\text{Ra} \rightarrow ^{210}\text{Pb}$, $^{210}\text{Pb} \rightarrow ^{206}\text{Pb}$ (^{238}U) were assumed to be in secular equilibrium.

The following “internal” sources were simulated in the $^{106}\text{CdWO}_4$ crystal scintillator:

- ^{40}K , $^{228}\text{Ra} \rightarrow ^{228}\text{Th}$, $^{228}\text{Th} \rightarrow ^{208}\text{Pb}$, $^{226}\text{Ra} \rightarrow ^{210}\text{Pb}$, and $^{210}\text{Pb} \rightarrow ^{206}\text{Pb}$ with activities estimated in the earlier stages of the experiment [45,46];
- distribution of α particles of ^{232}Th and ^{238}U with their daughters not discarded by the pulse-shape analysis;
- two-neutrino double beta decay of ^{116}Cd with the half-life $T_{1/2} = 2.63 \times 10^{19}$ yr [47].

The following “external” sources were simulated in the materials of the set-up:

- ^{40}K , $^{228}\text{Ra} \rightarrow ^{228}\text{Th}$, $^{228}\text{Th} \rightarrow ^{208}\text{Pb}$, $^{226}\text{Ra} \rightarrow ^{210}\text{Pb}$ in the internal and external copper details, the quartz light guides, the PbWO₄ crystal light-guide, the PMTs;
- $^{210}\text{Pb} \rightarrow ^{206}\text{Pb}$ in the PbWO₄ crystal light-guide;
- $^{228}\text{Th} \rightarrow ^{208}\text{Pb}$ and $^{226}\text{Ra} \rightarrow ^{210}\text{Pb}$ in the CdWO₄ crystal scintillators;
- ^{56}Co and ^{60}Co in the internal copper bricks.

The background components were simulated using the EGSnrc package with initial kinematics given by the DECAY0 event generator [48]. The distribution of residual α particles of ^{232}Th and ^{238}U with their daughters was constructed from the experimental data by using the pulse-shape analysis.

The simulated models were used to fit the energy spectra of γ and β events in anti-coincidence with the CdWO₄ counters and in coincidence with event(s) in at least one of the CdWO₄ counters with the energy release $E = 511 \pm 2\sigma$ keV. The data were fitted in the energy intervals (940–4000) keV (anti-coincidence data) and (240–3940) keV (coincidence with 511 keV). The fit quality is reasonable ($\chi^2 = 457$ for 235 degrees of freedom). The results of the fit and the main components of the background are shown in Fig. 7.

The fit allowed to estimate limits on radioactive contamination of the materials of the low-background set-up. The data are presented in Table 1.

3.2. Limits on 2EC, EC β^+ and 2 β^+ processes in ^{106}Cd

There are no peculiarities in the experimental data that could be ascribed to 2 β processes in ^{106}Cd . Lower limits on the half-life of ^{106}Cd relatively to different 2 β decay channels and modes can be estimated by using the following formula:

¹ Secular equilibrium in the ^{232}Th and ^{238}U decay families (when activities of daughter nuclides are equal to the activity of their parent nuclide) is typically broken in almost all materials due to physical or chemical processes utilized in the material production (see, e.g., [42–44]).

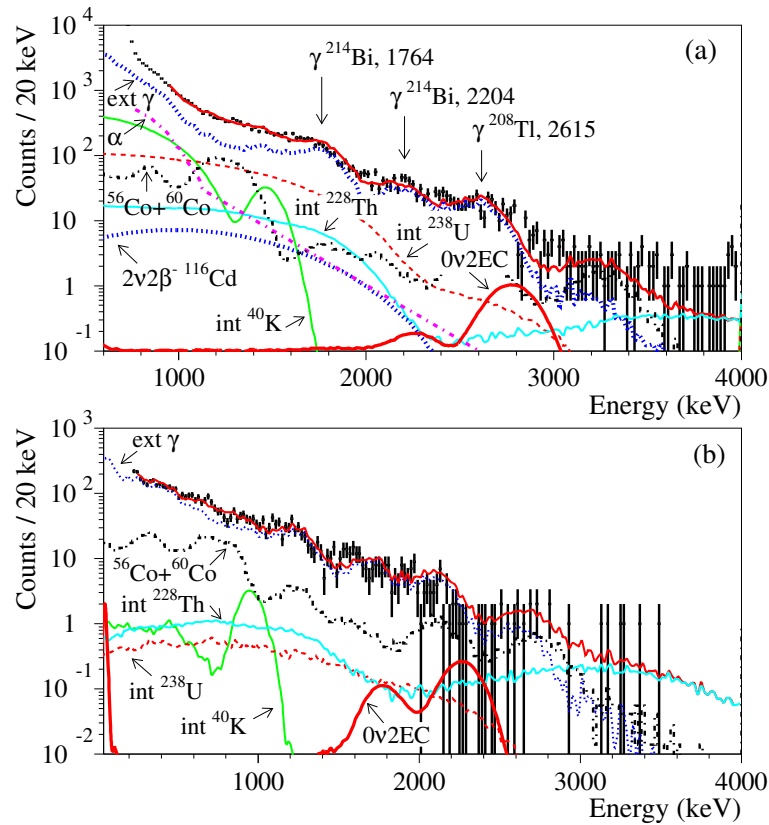


Figure 7. Energy spectra of the γ and β events accumulated for 26033 h by the $^{106}\text{CdWO}_4$ scintillation detector in anti-coincidence with the CdWO_4 counters (a) and in coincidence with the 511 keV annihilation γ quanta in at least one of the CdWO_4 counters (b) (points) together with the background model (red line). The main components of the background are shown: the distributions of internal contaminations ("int ^{40}K ", "int ^{232}Th ", and "int ^{238}U ") and external γ quanta ("ext γ "), residual α particles in the $^{106}\text{CdWO}_4$ crystal (α), cosmogenic ^{56}Co and ^{60}Co in the copper shield details, the $2\nu 2\beta$ decay of ^{116}Cd . The excluded distributions of the $0\nu 2\text{EC}$ decay of ^{106}Cd to the ground state of ^{106}Pd with the half-life $T_{1/2} = 6.8 \times 10^{20}$ yr are shown by red solid line.

$$\lim T_{1/2} = N \cdot \ln 2 \cdot \eta_{\text{det}} \cdot \eta_{\text{sel}} \cdot t / \lim S, \quad (2)$$

where N is the number of ^{106}Cd nuclei in the $^{106}\text{CdWO}_4$ crystal (2.42×10^{23}), η_{det} is the detection efficiency for the process of decay (calculated as a ratio of the events number in a simulated distribution to the number of generated events), η_{sel} is the selection cuts efficiency (selection by PSD, time coincidence, energy interval), t is the time of measurements, and $\lim S$ is the number of events of the effect searched for, which can be excluded at a given confidence level (C.L.). The responses of the detector system to different modes and channels of ^{106}Cd double beta decay were simulated using the EGSnrc package with initial kinematics given by the DECAY0 event generator. About 5×10^6 events were generated for each decay channel.

Different data were analyzed to estimate limits on the 2β processes in ^{106}Cd . Fit of the anti-coincidence spectrum by the above described model plus a simulated distribution of the $0\nu 2\text{EC}$ decay of ^{106}Cd to the ground state of ^{106}Pd returns the area of the distribution (205 ± 99) counts that is no evidence for the effect searched for. According to [49] we took 367 events as $\lim S$ at 90% C.L.² The detection efficiency for the decay was simulated as $\eta_{\text{det}} = 0.522$. Taking into account the selection cut efficiency due to application of the PSD to select γ and β events $\eta_{\text{sel}} = 0.955$, we got a lower limit on the half-life of ^{106}Cd relative to the $0\nu 2\text{EC}$ decay to the ground state of ^{106}Pd $T_{1/2} \geq 6.8 \times 10^{20}$ yr (the excluded distribution of the $0\nu 2\text{EC}$ decay is shown in Fig. 7). The limit is slightly worse than the one obtained in the previous stage of the experiment ($T_{1/2} \geq 1.0 \times 10^{21}$ yr [21], see also Table 2).

Fit of the $^{106}\text{CdWO}_4$ detector data in coincidence with signal(s) in the CdWO_4 counters by the above described background model was more sensitive to the most of the modes and channels of the decay searched for. An example of such an analysis for the $0\nu\text{EC}\beta^+$ and $0\nu 2\beta^+$ decays of ^{106}Cd to the ground state of ^{106}Pd by using the data measured with the $^{106}\text{CdWO}_4$ detector in coincidence with 511 keV events in at least one of the CdWO_4 counters is shown in Fig. 8. The selection cuts efficiency, e.g., for the $0\nu\text{EC}\beta^+$ process was calculated to be $\eta_{\text{sel}} = 0.909$ as a product of the PSD to select γ and β events in the interval $\pm 2\sigma$ of the mean time values (0.9546), the time coincidence efficiency in the interval $\pm 3\sigma$ (0.9973), the energy interval $\pm 2\sigma$ to select 511 keV events in the CdWO_4 counters (0.9545). The data on the efficiencies, values of $\lim S$ and the obtained half-life limits are given in Table 2.

Another example is search for $0\nu 2\text{EC}$ transition of ^{106}Cd to the 2718 keV excited level of ^{106}Pd (considered as one of the most promising decay channels from the point of view of a possible resonant process [14]). The search was realized by analysis of the $^{106}\text{CdWO}_4$ detector data in coincidence with event(s) in at least one of the CdWO_4 counters in the energy interval $(1046 - 1.5\sigma) - (1160 + 1.7\sigma)$ keV. The interval should contain two intensive γ quanta with energies 1046 keV and 1160 keV expected in the decay searched for (see the decay scheme in Fig. 1). The spectrum and its fit, consisting of the background model and excluded distribution of the resonant process searched for, is presented in Fig. 9.

The highest sensitivity to several decay channels with positron(s) emission was achieved by using the data gathered by the $^{106}\text{CdWO}_4$ detector in coincidence with 511 keV annihilation γ quanta in both of the CdWO_4 counters thanks to a rather high detection efficiency of the CdWO_4 counters and a very low background counting rate (see Fig. 10). However, the fit of the spectrum by the background components is not reliable enough due to a very low statistics of the data. Thus, the method of comparison of the measured background with the expected one was applied for the analysis. The expected background was estimated from the results of the fit shown in Fig. 7. There are 54 counts in the whole spectrum, while the estimated background is 55.3 counts confirming a correct background modelling. In the energy interval

² In the present work all the limits are given with 90% C.L. Only statistical errors coming from the data fluctuations were taken into account in the estimations of the $\lim S$ values, and systematic contributions have not been included in the half-life limit values.

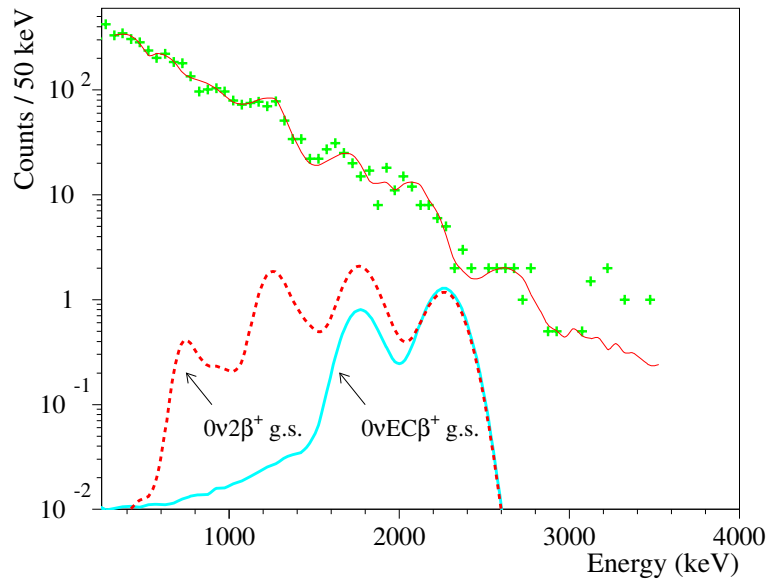


Figure 8. Energy spectrum of the γ and β events measured for 26033 h by the $^{106}\text{CdWO}_4$ detector in coincidence with events in at least one of the CdWO_4 counters with energy $E = 511 \pm 2\sigma$ keV (crosses). The solid red line shows the fit of the data by the background model (see Sec. 3.1). Excluded distributions of $0\nu\text{EC}\beta^+$ and $0\nu2\beta^+$ decays of ^{106}Cd to the ground state of ^{106}Pd with the half-lives $T_{1/2} = 1.4 \times 10^{22}$ yr and $T_{1/2} = 5.9 \times 10^{21}$ yr, respectively, are shown.

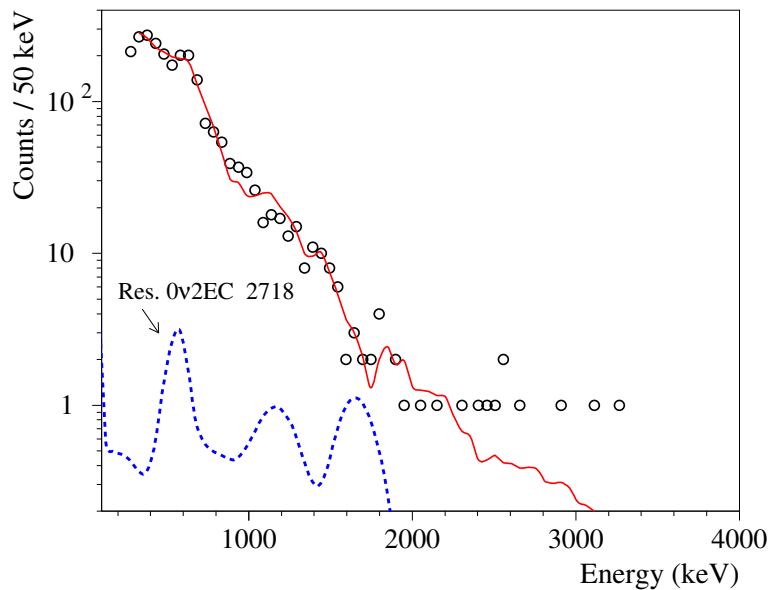


Figure 9. Energy spectrum of γ and β events measured by the $^{106}\text{CdWO}_4$ detector for 26033 h in coincidence with event(s) in at least one of the CdWO_4 counters in the energy interval $(1046 - 1.5\sigma) - (1160 + 1.7\sigma)$ keV (circles) and its fit by the model of background (red line). The excluded distribution of a possible resonant $0\nu2\text{EC}$ decay of ^{106}Cd to the 2718 keV excited level of ^{106}Pd with the half-life $T_{1/2} = 2.9 \times 10^{21}$ yr is shown.

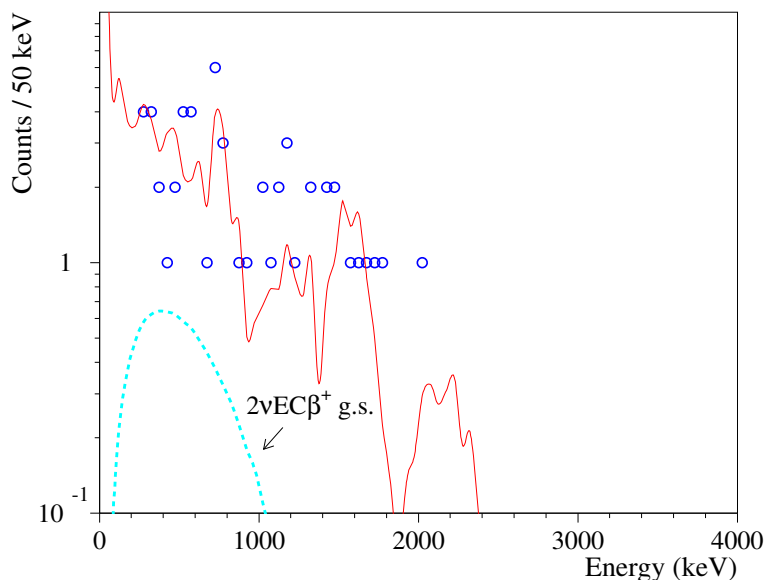


Figure 10. Energy spectrum of γ and β events measured by the $^{106}\text{CdWO}_4$ detector for 26033 h in coincidence with 511 keV annihilation γ quanta in both of the CdWO_4 counters (circles). The expected background, built on the basis of the fit presented in Fig. 7, is shown by red solid line. The excluded distribution of the $2\nu\text{EC}\beta^+$ decay of ^{106}Cd to the ground state of ^{106}Pd with the half-life $T_{1/2} = 2.1 \times 10^{21}$ yr is shown.

(250–1000) keV the measured background is 33 counts, while the estimated one is 37.4 counts that leads to $\text{lim } S = 6.7$ counts in accordance with the recommendations [49]. Taking into account the detection and the selections efficiencies for the $2\nu\text{EC}\beta^+$ decay of ^{106}Cd to the ground state of ^{106}Pd (0.040 and 0.703, respectively) one can get a half-life limit $T_{1/2} = 2.1 \times 10^{21}$ yr that is about two times higher than the limit ($T_{1/2} = 1.1 \times 10^{21}$ yr) obtained in the previous stage of the experiment [34].

Limits on other 2β decay processes in ^{106}Cd were obtained in a similar way. They are presented in Table 2, where the results of the most sensitive previous experiments are given for comparison.

A limit on effective nuclear matrix elements for the $2\nu\text{EC}\beta^+$ decay of ^{106}Cd to the ground state of ^{106}Pd could be estimated by using the calculations of the phase-space factors for the decay [50,51] with the formula $1/T_{1/2} = G^{2\nu\text{EC}\beta^+} \times |M^{eff}|^2$. The effective matrix nuclear element M^{eff} is expressed by $M^{eff} = g_A^2 \times M^{2\nu\text{EC}\beta^+}$, where g_A is the axial-vector coupling constant, $M^{2\nu\text{EC}\beta^+}$ is nuclear matrix element. An upper limit on the value of the effective matrix nuclear element for the process can be estimated as $M^{eff} \leq (0.80 - 0.82)$.

The half-life limit on the $2\nu\text{EC}\beta^+$ decay of ^{106}Cd to the ground state of ^{106}Pd , $T_{1/2} \geq 2.1 \times 10^{21}$ yr, approaches the region of the theoretical predictions that are in the range $10^{21} - 10^{22}$ yr [10,52–55]. The sensitivity to the double beta decay processes in ^{106}Cd is expected to be improved in the currently running experiment with reduced background thanks to utilization of ultra-radiopure PMTs, longer quartz light-guides for the CdWO_4 counters, a more powerful passive shield of the detector system. Also the energy resolution of the $^{106}\text{CdWO}_4$ detector was improved, roughly by a factor ~ 1.8 , thanks to replacement of the PbWO_4 light-guide by a plastic scintillator light-guide with a substantially better optical transmittance. This replacement became possible due to an extremely low radioactive contamination of the specially developed R11065-20 MOD Hamamatsu PMT [56] used for the $^{106}\text{CdWO}_4$ detector.

Table 2. Half-life limits on 2β processes in ^{106}Cd . The experimental selection is also reported (AC, anti-coincidence; CC, in coincidence, at the given energy (energies) with CdWO_4 ; CC 511&511, in coincidence with energies 511 keV in both of the CdWO_4 counters). η_{det} denotes the detection efficiency, η_{sel} is the selection cuts efficiency. The results of the most sensitive previous experiments are given for comparison.

Decay, level of ^{106}Pd	Exp. selection	η_{det}	η_{sel}	lim S	lim $T_{1/2}$ (yr) at 90% C.L.	
					Present work	Best previous
$2\nu 2\text{EC } 2^+ 1128$	CC 616	0.135	0.909	92	$\geq 6.6 \times 10^{20}$	$\geq 5.5 \times 10^{20}$ [34]
$2\nu 2\text{EC } 0^+ 1134$	CC 622	0.188	0.909	86	$\geq 9.9 \times 10^{20}$	$\geq 1.0 \times 10^{21}$ [34]
$2\nu 2\text{EC } 2^+ 1562$	CC 1050	0.138	0.909	80	$\geq 7.8 \times 10^{20}$	$\geq 7.4 \times 10^{20}$ [34]
$2\nu 2\text{EC } 0^+ 1706$	CC 1194	0.134	0.909	90	$\geq 6.7 \times 10^{20}$	$\geq 7.1 \times 10^{20}$ [34]
$2\nu 2\text{EC } 0^+ 2001$	CC 873	0.153	0.909	46	$\geq 1.5 \times 10^{21}$	$\geq 9.7 \times 10^{20}$ [34]
$2\nu 2\text{EC } 0^+ 2278$	CC 1766	0.091	0.909	131	$\geq 3.1 \times 10^{20}$	$\geq 1.0 \times 10^{21}$ [34]
$0\nu 2\text{EC g.s.}$	AC	0.522	0.955	367	$\geq 6.8 \times 10^{20}$	$\geq 1.0 \times 10^{21}$ [21]
$0\nu 2\text{EC } 2^+ 512$	AC	0.319	0.955	443	$\geq 3.4 \times 10^{20}$	$\geq 5.1 \times 10^{20}$ [21]
$0\nu 2\text{EC } 2^+ 1128$	CC 616	0.118	0.909	110	$\geq 4.9 \times 10^{20}$	$\geq 5.1 \times 10^{20}$ [34]
$0\nu 2\text{EC } 0^+ 1134$	CC 622	0.155	0.909	109	$\geq 6.4 \times 10^{20}$	$\geq 1.1 \times 10^{21}$ [34]
$0\nu 2\text{EC } 2^+ 1562$	CC 1050	0.136	0.909	45	$\geq 1.4 \times 10^{21}$	$\geq 7.3 \times 10^{20}$ [34]
$0\nu 2\text{EC } 0^+ 1706$	CC 1194	0.120	0.909	27	$\geq 2.0 \times 10^{21}$	$\geq 1.0 \times 10^{21}$ [34]
$0\nu 2\text{EC } 0^+ 2001$	CC 873	0.135	0.909	177	$\geq 3.5 \times 10^{20}$	$\geq 1.2 \times 10^{21}$ [34]
$0\nu 2\text{EC } 0^+ 2278$	CC 1766	0.079	0.909	29	$\geq 1.2 \times 10^{21}$	$\geq 8.6 \times 10^{20}$ [34]
Res. $0\nu 2\text{K } 2718$	CC 1046 + 1160	0.215	0.909	33	$\geq 2.9 \times 10^{21}$	$\geq 1.1 \times 10^{21}$ [34]
Res. $0\nu \text{KL}_1 4^+ 2741$	AC	0.454	0.952	663	$\geq 3.2 \times 10^{20}$	$\geq 9.5 \times 10^{20}$ [21]
Res. $0\nu \text{KL}_3 2,3^- 2748$	AC	0.318	0.955	432	$\geq 3.5 \times 10^{20}$	$\geq 1.4 \times 10^{21}$ [34]
$2\nu \text{EC}\beta^+ \text{ g.s.}$	CC 511&511	0.040	0.703	6.7	$\geq 2.1 \times 10^{21}$	$\geq 1.1 \times 10^{21}$ [34]
$2\nu \text{EC}\beta^+ 2^+ 512$	CC 511&511	0.047	0.459	4.0	$\geq 2.7 \times 10^{21}$	$\geq 1.3 \times 10^{21}$ [34]
$2\nu \text{EC}\beta^+ 2^+ 1128$	CC 511&511	0.029	0.509	5.6	$\geq 1.3 \times 10^{21}$	$\geq 1.0 \times 10^{21}$ [34]
$2\nu \text{EC}\beta^+ 0^+ 1134$	CC 511&511	0.031	0.603	11	$\geq 8.5 \times 10^{20}$	$\geq 1.1 \times 10^{21}$ [34]
$0\nu \text{EC}\beta^+ \text{ g.s.}$	CC 511	0.376	0.909	12	$\geq 1.4 \times 10^{22}$	$\geq 2.2 \times 10^{21}$ [21]
$0\nu \text{EC}\beta^+ 2^+ 512$	CC 511	0.384	0.909	18	$\geq 9.7 \times 10^{21}$	$\geq 1.9 \times 10^{21}$ [34]
$0\nu \text{EC}\beta^+ 2^+ 1128$	CC 511	0.314	0.909	14	$\geq 1.0 \times 10^{22}$	$\geq 1.3 \times 10^{21}$ [34]
$0\nu \text{EC}\beta^+ 0^+ 1134$	CC 511&511	0.030	0.385	5.0	$\geq 1.2 \times 10^{21}$	$\geq 1.9 \times 10^{21}$ [34]
$2\nu 2\beta^+ \text{ g.s.}$	CC 511&511	0.052	0.385	5.8	$\geq 1.7 \times 10^{21}$	$\geq 2.3 \times 10^{21}$ [34]
$2\nu 2\beta^+ 2^+ 512$	CC 511&511	0.048	0.323	3.4	$\geq 2.3 \times 10^{21}$	$\geq 2.5 \times 10^{21}$ [34]
$0\nu 2\beta^+ \text{ g.s.}$	CC 511	0.391	0.909	30	$\geq 5.9 \times 10^{21}$	$\geq 3.0 \times 10^{21}$ [34]
$0\nu 2\beta^+ 2^+ 512$	CC 511	0.370	0.909	39	$\geq 4.0 \times 10^{21}$	$\geq 2.5 \times 10^{21}$ [34]

4. Conclusions

The experiment to search for double beta decay of ^{106}Cd with enriched $^{106}\text{CdWO}_4$ scintillator in coincidence with two large volume CdWO_4 scintillation counters was performed at the Gran Sasso underground laboratory of INFN (Italy). New improved limits are set on the different channels of ^{106}Cd double beta decay at level of $10^{20} - 10^{22}$ yr. The new improved limit on half-life of ^{106}Cd relative to the $2\nu\text{EC}\beta^+$ decay was estimated as $T_{1/2} \geq 2.1 \times 10^{21}$ yr. The sensitivity is within the region of the theoretical predictions for the decay probability that are in the range of $T_{1/2} \sim 10^{21} - 10^{22}$ yr. A new improved limit was set for the resonant neutrinoless double-electron capture to the 2718 keV excited level of ^{106}Pd as $T_{1/2}^{0\nu 2K} \geq 2.9 \times 10^{21}$ yr.

The next stage of experiment is running at LNGS in the DAMA/R&D set-up with an improved sensitivity to all the decay channels thanks to reduction of the background approximately by a factor 3–5 with utilization of ultra-radiopure PMTs, longer quartz light-guides for the CdWO_4 counters, a more powerful passive shield of the detector system. The energy resolution of the $^{106}\text{CdWO}_4$ detector was improved too thanks to replacement of the PbWO_4 light-guide by a plastic scintillator light-guide with a substantially better optical transmittance. As a result, the sensitivity to the $2\nu\text{EC}\beta^+$ decay of ^{106}Cd is expected to be high enough to detect the process with the half-life at level of $\sim (0.5 - 1) \times 10^{22}$ yr over 5 yr of measurements.

5. Acknowledgments

D.V.K. and O.G.P. were supported in part by the project “Investigation of double beta decay, rare alpha and beta decays” of the program of the National Academy of Sciences of Ukraine “Laboratory of young scientists” Grant No. 0120U101838. F.A.D., D.V.K., V.R.K., V.V.K., V.I.T. and M.M.Z. were supported in part by the project “Double beta decay” of the National Research Foundation of Ukraine Grant No. 2020.02/0011. F.A.D. greatly acknowledges the Government of Ukraine for the quarantine measures that have been taken against the Coronavirus disease 2019 that substantially reduced much unnecessary bureaucratic work.

Conflicts of Interest: The authors declare no conflict of interest.

References

- Giuliani, A.; Poves, A. Neutrinoless Double-Beta Decay. *AHEP* **2012**, *2012*, 857016.
- Cremonesi, O.; Pavan, M. Challenges in Double Beta Decay. *AHEP* **2014**, *2014*, 951432.
- Vergados, J.D.; Ejiri, H.; Šimkovic, F. Neutrinoless double beta decay and neutrino mass. *Int. J Mod. Phys. E* **2016**, *25*, 1630007.
- Bilenky, S.M.; Giunti, C. Neutrinoless double-beta decay: A probe of physics beyond the Standard Model. *Int. J Mod. Phys. A* **2015**, *30*, 1530001.
- Dell’Oro, S.; Marcocci, S.; Viel, M.; Vissani, F. Neutrinoless Double Beta Decay: 2015 Review. *AHEP* **2016**, *2016*, 2162659.
- Dolinski, M.J.; Poon, A.W.P.; Rodejohann, W. Neutrinoless double beta decay: Status and prospects. *Annu. Rev. Nucl. Part. Sci.* **2019**, *69*, 219–251.
- Asaka, T.; Shaposhnikov, M. The νMSM , dark matter and baryon asymmetry of the universe. *Phys. Lett. B* **2005**, *620*, 17–26.
- Deppisch, F.F.; Graf, L.; Harz, J.; Huang, W.C. Neutrinoless double beta decay and the baryon asymmetry of the Universe. *Phys. Rev. D* **2018**, *98*, 055029.
- Barabash, A.S. Precise Half-Life Values for Two-Neutrino Double- β Decay: 2020 Review. *Universe* **2020**, *6*, 159.
- Hirsch, M.; Muto, K.; Oda, T.; Klapdor-Kleingrothaus, H.V. Nuclear structure calculation of $\beta^+\beta^+$, $\beta^+\text{EC}$, and EC/EC decay matrix elements. *Z. Phys. A* **1994**, *347*, 151–160.

11. Winter, R. Double K capture and single K capture with positron emission. *Phys. Rev.* **1955**, *100*, 142–144.
12. Voloshin, M.B.; Mitselmakher, G.V.; Eramzhyan, R.A. Conversion of an atomic electron into a positron and double β^+ decay. *JETP Lett.* **1982**, *35*, 656–659.
13. Bernabeu, J.; De Rujula, A.; Jarlskog, C. Neutrinoless double electron capture as a tool to measure the electron neutrino mass. *Nucl. Phys. B* **1983**, *223*, 15–28.
14. Krivoruchenko, M.I.; Šimkovic, F.; Frekers, D.; Faessler, F. Resonance enhancement of neutrinoless double electron capture. *Nucl. Phys. A* **2011**, *859*, 140–171.
15. Meshik, A.P.; Hohenberg, C.M.; Pravdivtseva, O.V.; Kapusta, Y.S. Weak decay of ^{130}Ba and ^{132}Ba : Geochemical measurements. *Phys. Rev. C* **2001**, *64*, 035205.
16. Pujol, M.; Marty, B.; Burnard, B.P.; Philippot, P. Xenon in Archean barite: Weak decay of ^{130}Ba , mass-dependent isotopic fractionation and implication for barite formation. *Geochim. Cosmochim. Acta* **2009**, *73*, 6834–6846.
17. Meshik, A.; Pravdivtseva, O. Weak Decay of Tellurium and Barium Isotopes in Geological Samples: Current Status. *JPS Conf. Proc.* **2017**, *14*, 020702.
18. Gavriilyuk, Y.M.; et al. Indications of $2\nu 2K$ capture in ^{78}Kr . *Phys. Rev. C* **2013**, *87*, 035501.
19. Ratkevich, S.S.; et al. Comparative study of the double-K-shell-vacancy production in single- and double-electron-capture decay. *Phys. Rev. C* **2017**, *96*, 065502.
20. XENON Collaboration. Observation of two-neutrino double electron capture in ^{124}Xe with XENON1T. *Nature* **2019**, *568*, 532–535.
21. Belli, P.; et al. Search for double- β decay processes in ^{106}Cd with the help of a $^{106}\text{CdWO}_4$ crystal scintillator. *Phys. Rev. C* **2012**, *85*, 044610.
22. Wang, M.; et al. The AME2016 atomic mass evaluation. *Chin. Phys. C* **2017**, *41*, 030003.
23. Meija, J.; et al. Isotopic compositions of the elements 2013 (IUPAC Technical Report). *Pure Appl. Chem.* **2016**, *88*, 293–306.
24. Kiel, H.; Münstermann, D.; Zuber, K. A search for various double beta decay modes of Cd, Te, and Zn isotopes. *Nucl. Phys. A* **2003**, *723*, 499–514.
25. Ebert, J.; et al. Current status and future perspectives of the COBRA experiment. *Adv. High Energy Phys.* **2013**, *2013*, 703572.
26. Ebert, J.; et al. Results of a search for neutrinoless double- β decay using the COBRA demonstrator. *Phys. Rev. C* **2016**, *94*, 024603.
27. Rukhadze, N.I.; et al. Search for double beta decay of ^{106}Cd . *Bull. Russ. Acad. Sci.: Phys.* **2011**, *75*, 879–882.
28. Rukhadze, N.I.; et al. New limits on double beta decay of ^{106}Cd . *Nucl. Phys. A* **2011**, *852*, 197–206.
29. Rukhadze, N.I.; et al. Search for double electron capture of ^{106}Cd . *Phys. At. Nuclei* **2006**, *69*, 2117–2123.
30. Rukhadze, N.I.; et al. Search for double beta decay of ^{106}Cd in the TGV-2 experiment. *J. Phys.: Conf. Ser.* **2016**, *718*, 062049.
31. Rukhadze, N.; on behalf of TGV collaboration. Search for double beta decay of ^{106}Cd with the TGV-2 spectrometer. *PoS* **2016**, *281*, 245.
32. Belli, P.; et al. Development of enriched $^{106}\text{CdWO}_4$ crystal scintillators to search for double β decay processes in ^{106}Cd . *Nucl. Instrum. Meth. A* **2010**, *615*, 301–306.
33. Laubenstein, M.; et al. Underground measurements of radioactivity. *Appl. Radiat. Isotopes* **2004**, *61*, 167.
34. Belli, P.; et al. Search for double- β decay in ^{106}Cd with an enriched $^{106}\text{CdWO}_4$ crystal scintillator in coincidence with four HPGe detectors. *Phys. Rev. C* **2016**, *93*, 045502.
35. Polischuk, O.G.; et al. New limit on two neutrino electron capture with positron emission in ^{106}Cd . *AIP Conf. Proc.* **2019**, *2165*, 020020.
36. De Frenne, D.; Negret, A. Nuclear data sheets for $A = 106$. *Nucl. Data Sheets* **2008**, *109*, 943–1102.
37. Boiko, R.S.; et al. Ultrapurification of archaeological lead. *Inorganic Materials* **2011**, *47*, 645–648.
38. Danevich, F.A.; et al. Ancient Greek lead findings in Ukraine. *Nucl. Instr. Meth. A* **2009**, *603*, 328–332.
39. Bernabei, R.; et al. First results from DAMA/LIBRA and the combined results with DAMA/NaI. *Eur. Phys. J. C* **2008**, *56*, 333–355.

40. Kawrakow, I.; Rogers, D.W.O. *The EGSnrc code system: Monte Carlo simulation of electron and photon transport*, NRCC Report PIRS-701, Ottawa; 2003.
41. Blachot, J. Nuclear data sheets for $A = 113$. *Nucl. Data Sheets* **2010**, *111*, 1471–1618.
42. Jagam, P.; Simpson, J.J. Measurements of Th, U and K concentrations in a variety of materials. *Nucl. Instr. Meth. A* **1993**, *324*, 389–398.
43. Righi, S.; Betti, M.; Bruzzi, L.; Mazzotti, G. Monitoring of natural radioactivity in working places. *Microchem. J.* **2000**, *67*, 119–126.
44. Danevich, F.A.; Tretyak, V.I. Radioactive contamination of scintillators. *Int. J. Mod. Phys. A* **2018**, *33*, 1843007.
45. Danevich, F.A.; et al. Development of radiopure cadmium tungstate crystal scintillators from enriched ^{106}Cd and ^{116}Cd to search for double beta decay. *AIP Conf. Proc.* **2013**, *1549*, 201–204.
46. Poda, D.V.; et al. CdWO_4 crystal scintillators from enriched isotopes for double beta decay experiments. *Radiat. Meas.* **2013**, *56*, 66–69.
47. Barabash, A.S.; et al. Final results of the Aurora experiment to study 2β decay of ^{116}Cd with enriched $^{116}\text{CdWO}_4$ crystal scintillators. *Phys. Rev. D* **98**, 2018, 092007.
48. Ponkratenko, O.A.; Tretyak, V.I.; Zdesenko, Y.G. Event generator DECAY4 for simulation of double-beta processes and decays of radioactive nuclei. *Phys. Atom. Nuclei* **2000**, *63*, 1282–1287.
49. Feldman, G.J.; Cousins, R.D. Unified approach to the classical statistical analysis of small signals. *Phys. Rev. D* **1998**, *57*, 3873–3889.
50. Kotila, J.; Iachello, F. Phase space factors for $\beta^+\beta^+$ decay and competing modes of double- β decay. *Phys. Rev. C* **2013**, *87*, 024313.
51. Mirea, M.; Pahomi, T.; Stoica, S. Values of the phase space factors involved in double beta decay. *Rom. Rep. Phys.* **2015**, *67*, 872–889.
52. Barabash, A.S.; et al. Theoretical and experimental investigation of the double beta processes in ^{106}Cd . *Nucl. Phys. A* **1996**, *604*, 115–128.
53. Toivanen, J.; Suhonen, J. Study of several double- β -decaying nuclei using the renormalized proton-neutron quasiparticle random-phase approximation. *Phys. Rev. C* **1997**, *55*, 2314–2323.
54. Romyantsev, O.A.; Urin, M.H. The strength of the analog and Gamow-Teller giant resonances and hindrance of the $2\nu\beta\beta$ -decay rate. *Phys. Lett. B* **1998**, *443*, 51–57.
55. Ejiri, H. Fermi surface quasi particle model nuclear matrix elements for two neutrino double beta decays. *J. Phys. G* **2017**, *44*, 115201.
56. Bernabei, R.; et al. Performances of the new high quantum efficiency PMTs in DAMA/LIBRA. *JINST* **2012**, *7*, 03009.